# Removal of methylene blue from aqueous solution using sediment obtained from a canal in an industrial park

Lih-Fu Chen, Hsiou-Hsuan Wang, Kao-Yung Lin, Jui-Yen Kuo, Ming-Kuang Wang and Cheng-Chung Liu

## ABSTRACT

Drainage canal sediments in an industrial park are generally dredged to landfill in Taiwan. The objective of this study was to evaluate feasibility employing the sediment as an adsorbent for removal of dye. The sediment contained approximately 10% of organic matter and little heavy metals. Infrared (IR) analysis revealed that carboxyl was the most important functional group for methylene blue (MB) sorption. Canal sediment could remove the most MB from water at pH 8.0 and this removal increased with increasing temperature. The MB sorption was well described by the Langmuir, Dubinin–Radushkevich, and Temkin sorption isotherms at 10 °C, but it showed good compliance with Freundlich isotherm at 25 °C and 40 °C. The MB adsorption was a spontaneous and endothermic reaction; its maximum calculated adsorption capacity ($Q_m$) was 56.0 mg $g^{-1}$ at 10 °C by the Langmuir isotherm. The calculated values of enthalpy ($\Delta H°$) and entropy ($\Delta S°$) are 14.6 kJ $mol^{-1}$ and 149.2 kJ $mol^{-1}$, respectively. Only pseudo-second-order adsorption kinetic model successfully described the kinetics of MB onto the sediment at different operation parameters. Activation energy of MB adsorption calculated from Arrhenius equation was 16.434 kJ $mol^{-1}$, indicating the binding between canal sediment and MB was a physical adsorption.

**Key words** | adsorption, canal sediment, Dubinin–Radushkevich, isotherms, kinetic, methylene blue

**Lih-Fu Chen**
College of Liberal Education,
Shu-Te University,
Kaohsiung 82445,
Taiwan

**Hsiou-Hsuan Wang**
Department of Materials Engineering,
National Ilan University,
Ilan 260,
Taiwan

**Kao-Yung Lin**
Department of Living Sciences,
Nation Open University,
Taipei 24701,
Taiwan

**Jui-Yen Kuo**
**Cheng-Chung Liu** (corresponding author)
Department of Environmental Engineering,
National Ilan University,
Ilan 260,
Taiwan
E-mail: *ccliu@niu.edu.tw*

**Ming-Kuang Wang**
Department of Agricultural Chemistry,
National Taiwan University,
Taipei 106,
Taiwan

## INTRODUCTION

Organic dyes are used widely as part of the coloring processes in textile, paper, plastics, leather tanning, food, polymer, cosmetics, printing, and dye manufacturing industries (Aroguz *et al.* 2008; Sham & Notley 2018). However, illegal and massive releases of dye wastewaters from textile industries into lakes and rivers have posed a serious risk to ecosystems. Highly colored dyes reduce light penetration and decrease photosynthesis (Waranusantigul *et al.* 2003). Some dyes are directly harmful to human health, having toxic, mutagenic, and carcinogenic effects (Chung & Cerniglia 1992).

Almost all dyes are poorly biodegradable or resistant to environmental conditions and therefore cause major problems in the treatment of wastewater from the dyeing industry. To purify effluent streams of dye, several physicochemical technologies, including chemical oxidation (Benjelloun *et al.* 2017), coagulation/flocculation (Mukhlish *et al.* 2016), membrane separation (Ma *et al.* 2017a, 2017b), ion exchange (Akazdam *et al.* 2017), electrochemical techniques (Gerçel 2016), photocatalysis (Molla *et al.* 2017), and adsorption (Mouni *et al.* 2018), have been proposed. Some highly toxic dyes are difficult to degrade by biological treatments. Thus, adsorption is of growing importance for removing pollutants from dye wastewaters (Sun & Yang 2003). Activated carbon is commonly used for dye removal in the field because of its effectiveness and high adsorption capacity. However, high operating costs and difficult generation limit its usage. In recent years, there has been increasing interest in identifying low-cost alternatives to activated carbon, such as magnetic $MnFe_2O_4$/clay nano

doi: 10.2166/wst.2018.326

composite (Nausheen *et al.* 2017), waste tire rubber (Islam *et al.* 2018), fish scale activated material (Marrakchi *et al.* 2017), agricultural wastes (Rebitanim *et al.* 2012; Bhatti *et al.* 2017; Shoukat *et al.* 2017), and biosorbents (Weng *et al.* 2009).

Methylene blue (MB), a heterocyclic basic dye that contains three water molecules in hydrated form ($C_{16}H_{18}N_3SCl \cdot 3H_2O$), is commonly employed for dying cotton, paper, silk, wood, and wool. It dissociates into MB cation and chloride in aqueous solutions. Although MB is not strongly hazardous, it may give rise to adverse effects on human health, including increased heart rate, respiratory sensitization, nausea, allergic dermatitis, dizziness, vomiting, and irritation of the gastrointestinal tract. It also causes convulsion, cyanosis, sweating, confusion, and short periods of difficult breathing on inhalation. Its degradation products in the body, such as toluidine, benzidine, and other aromatic components, may cause cancer and mutations (Reddy *et al.* 2016). Nevertheless, MB is difficult to remove from wastewater by biological treatment or chemical precipitation processes (Franca *et al.* 2009).

Liu *et al.* (2012a) demonstrated that wine-processing waste sludge (WPWS) enabled adsorption of high amounts of MB from aqueous solution (maximum adsorption capacity ($Q_m$) = 285.7 mg $g^{-1}$) by means of its high organic contents. This characteristic makes this sludge excellent for adsorbing dyes due to its large surface area and high binding affinity. Drainage canal sediments in an industrial park, Taiwan, appear very similar to WPWS. These sediments also have a black color and fine texture. In fact, the canal sediment is composed of silt and very fine sand that is covered with black, sticky organic materials. Thus, the sediment may be a good candidate for an adsorbent for MB removal.

When the canal water flows slowly through the industrial area, it receives a quantity of domestic sewage that has a high biochemical oxygen demand level. In addition, numerous waste effluents are discharged without any treatment from illegal metal-processing factories. When these dissolving organic materials decompose and settle to the bottom of the canal, they become sticky, humus-like matter that coats the minerals. Therefore, the high organic content of this material suggested to us that it could be used as a low-cost adsorbent. Most of these canal sediments are sent to a landfill for final disposal. The rest is sent to a brickfield or cement plant in Taiwan; the Si, Al, and Ca in the canal sediments can be used as raw materials of cement. We considered that the canal sediment could be reused for the removal of dye from textile wastewaters before its final disposal.

The objective of this work was to evaluate the feasibility of using the canal sediment as an adsorbent for wastewater treatment by the toxic characteristic leaching procedure (TCLP) test and the test of heavy metal dissolution. The effects of pH, initial MB concentration, temperature, and particle size on MB adsorption were investigated. Data from isotherm and kinetic studies were processed employing several models to explore the mechanism between canal sediment and MB. The pseudo-first-order, pseudo-second-order, and Elovich models were introduced to correlate the adsorption kinetics data. Equilibrium data were analyzed using the Langmuir, Freundlich, Temkin, and Dubinin–Radushkevich isotherm models and the adsorption thermodynamics were evaluated. The best operational parameters would be proposed for application in the treatment of dye-containing wastewaters.

## MATERIALS AND METHODS

### Sample preparation and characterization of canal sediment

The sediment was obtained using an Ekman dredge from a canal in a medium industrial area in Luzhou District, New Taipei City, Taiwan (TWD97: 296509, 2776633). The dark color of the canal water at this location implied that the sediment was rich in organic material, which is beneficial to dye adsorption. The sediment recovered was dried at room temperature. Then, it was ground and sieved into four particle size ranges, 50–100, 100–140, 140–200, and 200–350 mesh sizes, which were represented by the average diameters of 0.297, 0.149, 0.105, and 0.105 mm, respectively. After sieving and collection, we found that the sediment with the 140–200 mesh size accounted for 70% of the original sediment. Therefore, this fraction was predominately employed for conducting the subsequent kinetic and isotherm experiments. The canal sediment was first examined by the TCLP test to determine whether it could be reused for other works. To find the relationship between pH and the dissolution of major toxic metals, 1 g of canal sediment (140–200 mesh) was mixed with 100 mL of aqueous solution of various pH values (i.e. 2.0, 3.0, 4.0, 5.0, 6.0, 7.0, 8.0, 9.0, and 10.0) at the constant speed of 100 rpm for 2 h at 25 °C. The suspensions were filtered through a 0.45-μm membrane filter. The concentrations of toxic metals in the filtrate were determined using an atomic absorption spectrophotometer.

A scanning electron microscope (JeoL JSM-7800F Prime, Japan) equipped with an energy-dispersive spectrometer (EDS) was employed to characterize the constituents and morphologies of the canal sediment. An elemental analyzer (EA) (Element vario EL cube, Germany) was also used for determination of other major elements. The pH of the canal sediment suspensions was measured at a 1:1 sediment-to-water ratio with a pH meter. The cation exchange capacity (CEC) of the canal sediment was determined by a conventional ammonium–sodium exchange method (Rhoades 1982). The organic matter of each fraction of the canal sediment was analyzed by the combustion method at 550 °C under the anaerobic condition using a programable controller furnace. For X-ray diffraction (XRD) determination, the canal sediment was pre-treated with 35% $H_2O_2$ solution to remove organic matter. Afterward, the air-dried sample was examined with Cu $K_\alpha$ radiation using a Rigaku TTRAX III powder diffraction meter (Rigaku, Tokyo, Japan) in the range of 4–50° (2θ) at a scanning speed of 1° (2θ) $min^{-1}$. The predominant functional groups of the canal sediment were characterized using a Fourier transform infrared (FT-IR) spectrometer (Bruker, Vertex 80v). All chemicals used in this investigation were analytical grade, and all solutions were prepared with deionized water. A stock MB solution (1,000 mg $L^{-1}$) was prepared from MB using deionized water and diluted to the desired concentrations. For the kinetic and isotherms experiments, all MB solutions were adjusted initially to pH 8.0 due to its best sorption. A mechanical shaker with adjustable agitation speed was used to conduct perfect mixing at 100 rpm.

## Kinetic experiments and models

To perform the kinetics experiments, 4.98 g of canal sediment was separately added to a series of 1,000-mL MB solutions with various temperatures (10, 25, 40, and 55 °C), MB concentrations (100, 200, 300, 400, and 500 mg $L^{-1}$), and particle sizes of canal sediment (50–100, 100–140, 140–200, and 200–350 mesh). MB was purchased from Riedel–de Haën (Germany, guaranteed analysis grade). The suspensions were agitated vigorously by the shaker for from 1.5 to 180 min. At the end of the desired time intervals, the proper volume of the mixed solutions was immediately filtered through a 0.45-μm membrane filter. The MB concentration in the filtrates was determined by a visible spectrophotometer at 664 nm. All kinetic experiments were conducted in duplicate at pH 8.0.

The adsorption kinetics of MB by the canal sediment at the different operating temperatures, initial MB concentrations, and canal sediment particle sizes were fitted using pseudo-first-order, pseudo-second-order, and Elovich adsorption equations. The pseudo-first-order equation was written as follows:

$$\log(q_e - q_t) = \log q_e - \frac{k_1}{2.303}t \quad (1)$$

where $k_1$ ($min^{-1}$) is the rate constant, $q_e$ (mg $g^{-1}$) is the amount adsorbed at equilibrium, and $q_t$ (mg $g^{-1}$) denotes the amount adsorbed at time t (min). The adsorption rate constant, $k_1$, can be obtained by plotting $\log(q_e - q_t)$ against $t$. The pseudo-second-order equation was written as

$$\frac{t}{q_t} = \frac{1}{k_2 q_e^2} + \frac{1}{q_e}t \quad (2)$$

where $k_2$ (g $mg^{-1}$ $min^{-1}$) is the rate constant. $k_2$ and $q_e$ can be calculated from the intercept and slope of a plot of $t/q_t$ against $t$.

## Adsorption experiments and isotherms

For the adsorption isotherms, 0.25 g of the canal sediment (140–200 mesh) was equilibrated separately with 50-mL solutions containing various MB concentrations (i.e. 100, 200, 300, 400, and 500 mg $L^{-1}$). The temperatures examined were 10, 25, 40, and 55 °C. After adjustment of the initial pH to 8.0 with either a 0.1 M NaOH or a 0.1 M HCl solution, the suspensions were shaken by the shaker with a constant speed of 100 rpm for 180 min. The suspensions were then filtered with a 0.45-μm filter membrane. The filtrates were analyzed for MB concentration at 664 nm using a visible spectrophotometer.

To determine the adsorption capacity of the canal sediment, an adsorption isotherm was carried out by analyzing the adsorption data fit to the models of the Langmuir, Freundlich, Temkin, and Dubinin–Radushkevich adsorption isotherm equations. The relative coefficients of these models were calculated using linear least-squares fitting. After linearization, the Langmuir adsorption isotherm equation of $((x/m) = (Qmk_LC_e)/(1 + k_LC_e))$ becomes

$$\frac{m}{x} = \frac{1}{X} = \frac{1}{Q_m} + \frac{1}{Qmk_L}\frac{1}{C_e} \quad (3)$$

The Langmuir constants $Q_m$ and $k_L$ are related to the maximum adsorption capacity and adsorption energy,

respectively. They can be determined from the intercept and slope of the linear plot of $1/X$ vs $1/C_e$.

The Freundlich isotherm equation $(x/m) = k_F C_e^{1/n}$ after linearization is

$$\log\left(\frac{x}{m}\right) = \log(X) = \log k_F + \frac{1}{n}\log C_e \tag{4}$$

where $X$ is the mass of adsorbed MB per mass of canal sediment (mg $g^{-1}$), $C_e$ is the equilibrium concentration of MB (mg $L^{-1}$), and $k_F$ and $n$ are constants of the Freundlich equation that represent adsorption capacity and intensity, respectively. Both $k_F$ and $n$ can be calculated from the slope and intercept of the linear plot of $\log(X)$ against $\log C_e$.

By ignoring the extremely high and low concentrations, the Temkin isotherm assumes that the heat of adsorption of all molecules in the layer would decrease with coverage linearly rather than logarithmically. This isotherm is characterized by a uniform distribution of binding energies, which can be obtained by plotting the adsorbed amount $q_e$ against $lnC_e$. The constant is determined from the slope and intercept. The model is given by the following equation:

$$q_e = \frac{RT}{b}\ln(A_T C_e) \tag{5}$$

where $A_T$ is the Temkin isotherm equilibrium binding constant (L $g^{-1}$), $b$ is the Temkin isotherm constant, $R$ is the universal gas constant (8.314 J $mol^{-1}$ $K^{-1}$), and $T$ is absolute temperature. The Temkin isotherm equation after linearization becomes

$$q_e = \frac{RT}{b_T}\ln A_T + \left(\frac{RT}{b}\right)\ln C_e \tag{6}$$

$$B = \frac{RT}{b_T}$$

$$q_e = B\ln A_T + B\ln C_e$$

where $B$ represents a constant related to the heat of sorption (J $mol^{-1}$).

The Dubinin–Radushkevich isotherm is another empirical model that is generally applied to express the adsorption mechanism with a Gaussian energy distribution onto both homogeneous and heterogeneous surfaces (Dabrowski 2001; Gunay *et al.* 2007). The model has often successfully fitted high solute activity and the intermediate range of concentrations data well. The non-linear expression of the Dubinin–Radushkevich isotherm model can be described by Equations (7) and (8):

$$q_e = q_s \exp(-K_{DR}\varepsilon^2) \tag{7}$$

$$\varepsilon = RT\ln\left(1 + \frac{1}{C_e}\right) \tag{8}$$

where $q_s$ (mg $g^{-1}$) is a constant in the Dubinin–Radushkevich isotherm model that is related to adsorption capacity, $K_{DR}$ ($mol^2/kJ^2$) is a constant related to the mean free energy of adsorption, $R$ (J mol $K^{-1}$) is the gas constant, $T$ ($K$) is the absolute temperature, and $C_e$ is the equilibrium concentration of MB (mg $L^{-1}$). After linearization, the Dubinin–Radushkevich isotherm equation becomes

$$\ln q_e = \ln q_s - (K_{DR}\varepsilon^2) \tag{9}$$

$$E = \frac{1}{\sqrt{2K_{DR}}}$$

where $E$ (K J $mol^{-1}$) is the mean free energy, the energy needed for removing an adsorbate molecule from the sorption site to infinity. The Dubinin–Radushkevich characteristic curve can be obtained by plotting $\ln q_e$ against $\varepsilon^2$, and $K_{DR}$ and $q_s$ are calculated by the slope and intercept, respectively.

## RESULTS AND DISCUSSION

### Characterization of the canal sediment

The sieved canal sediment particles had a dark color, indicating that the sediment contained abundant humus-like materials. SEM micrographs at 2,500× and 10,000× magnification showed that the canal sediment exhibits the morphology of a roughly textured surface (Figure 1). When an adsorbent has a rough surface, it implies that the adsorbent has a higher specific surface area, which is beneficial to adsorption. The XRD spectrum depicted the two strongest peaks at 0.43 nm and 0.334 nm, respectively, which were assigned to quartz (Figure 2). This reveals that quartz is the major mineral in the sediment. In addition, small amounts of mica (peak at 1.00 nm) and kaolinite (peak at 0.71 nm) were found in the canal sediment. As listed in Table 1, dissolution of only Cu, Ni, and Zn was observed in the TCLP test. The Cu dissolution amount was lower than the standard level; however, the standard level has not yet been defined for Ni and Zn. This result supported the suitability of the

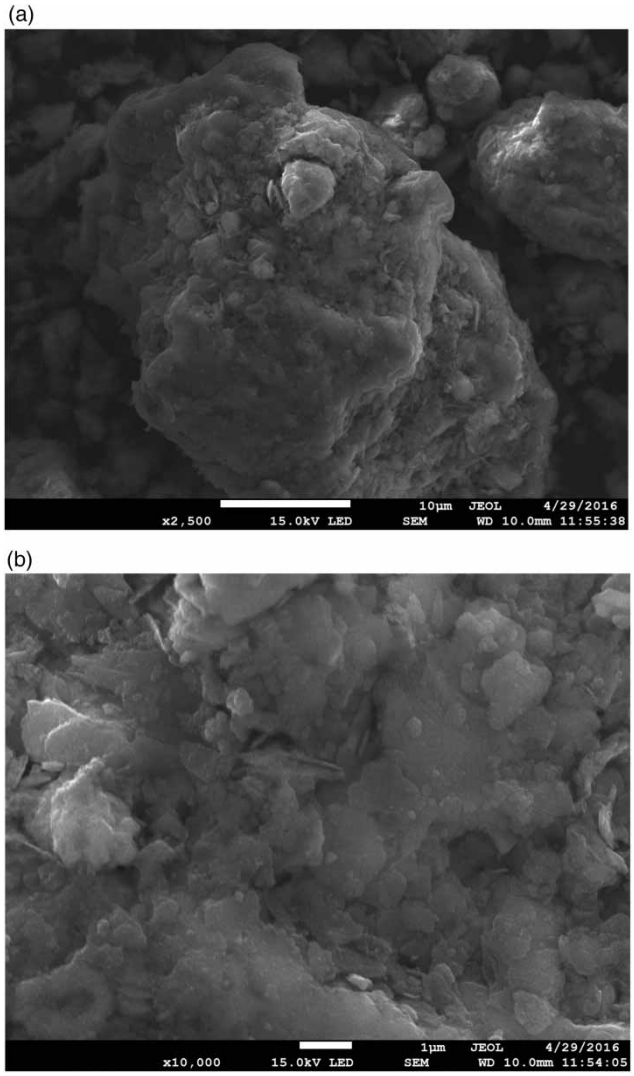


**Figure 1** | SEM micrographs of canal sediment (140–200 mesh) at different magnifications: (a) 2,500× and (b) 10,000×.

canal sediment for reuse in other works. Both the EDS and EA analyses revealed that Si (20.2%), O (39.5%), Fe (11.6%), Al (8.95%), C (6.16%), K (2.99%), Ca (2.88%), Mn (1.42%), H (1.32%), Na (1.22%), Cl (1.13%), and S (1.09%) are the dominant elements in the canal sediment. Additionally, N, P, Cr, and Ti have relatively low abundances in the sediment, with amounts lower than 1.00%. The high contents of Si, O, Fe, and Al indicate that the main content of the canal sediment consists of fine quartz sand and iron and aluminum oxides. The pH and CEC levels of the canal sediment were 7.4 and 33.2 $cmol_c\ kg^{-1}$, respectively. The organic matter content of the sediment was estimated as approximately 10%. Textural analysis indicated that the clay, silt, and sand contents of the original canal sediment were 2%, 40%, and 58%, respectively.

The sediment also contained small amounts of heavy metals because the canal receives wastewater discharged from plating, alloy, and tannery factories in the industrial park. Their concentrations were the following: Cr (875 ppm), Cu (1,438 ppm), Zn (683 ppm), Ni (515 ppm), Cd (0.95 ppm), Pb (116 ppm), and Hg (0.949 ppm). Clearly, the contents of Cr, Cu, Ni, and Zn in the sediment are substantially higher than the EPA sediment standard values in Taiwan. Thus, it was necessary to determine whether these metals would dissolve during the MB adsorption process. As shown in Table 2, a significant dissolution of Cu, Ni, and Zn occurs at pH 2.0 and the dissolution amounts are higher than the discharge standard. However, the dissolution abruptly decreases when the pH level is increased to 3.0; all dissolution amounts become insignificant and far below the standard levels. When the reactions were performed at pH higher than 4.0, only a small amount of Cu dissolved ($<0.05\ mg\ L^{-1}$). Thus, we confirmed that this sediment can be used as an adsorbent when conducting MB adsorption under a neutral or alkaline condition.

As shown in Figure 3, an intense FT-IR absorption band at $988\ cm^{-1}$ is attributable to the Si–O–Si stretching of quartz (White & Roth 1982). Quartz was the major component of the sand in the sediment. A medium FT-IR absorption band at $2{,}923\ cm^{-1}$ was assigned to the asymmetric vibration of $CH_2$ (Gerasimowicz & Byler 1985). Another FT-IR band appearing at around $1{,}640\ cm^{-1}$ was recognized as the asymmetric stretching band of carboxyl, which originated from the organic materials coating the sand (Hagvall *et al.* 2015). A trough at $1{,}420\ cm^{-1}$ was ascribed to aryl structures (Miralles *et al.* 2012). We are convinced that carboxyl was the main functional group forming a complex with MB. The adsorption mechanism at pH 8.0 can be expressed as follows:

$$R - COO^- + MB^+ \rightarrow R - COO - MB$$

## Effect of pH on MB sorption

The maximum removal efficiency of MB sorption occurred in the high pH range (Figure 4). Additionally, massive proton dissociation from carboxyl groups enhanced the increase of negatively charged sites on the canal sediment, resulting in a higher MB adsorption. However, all of the

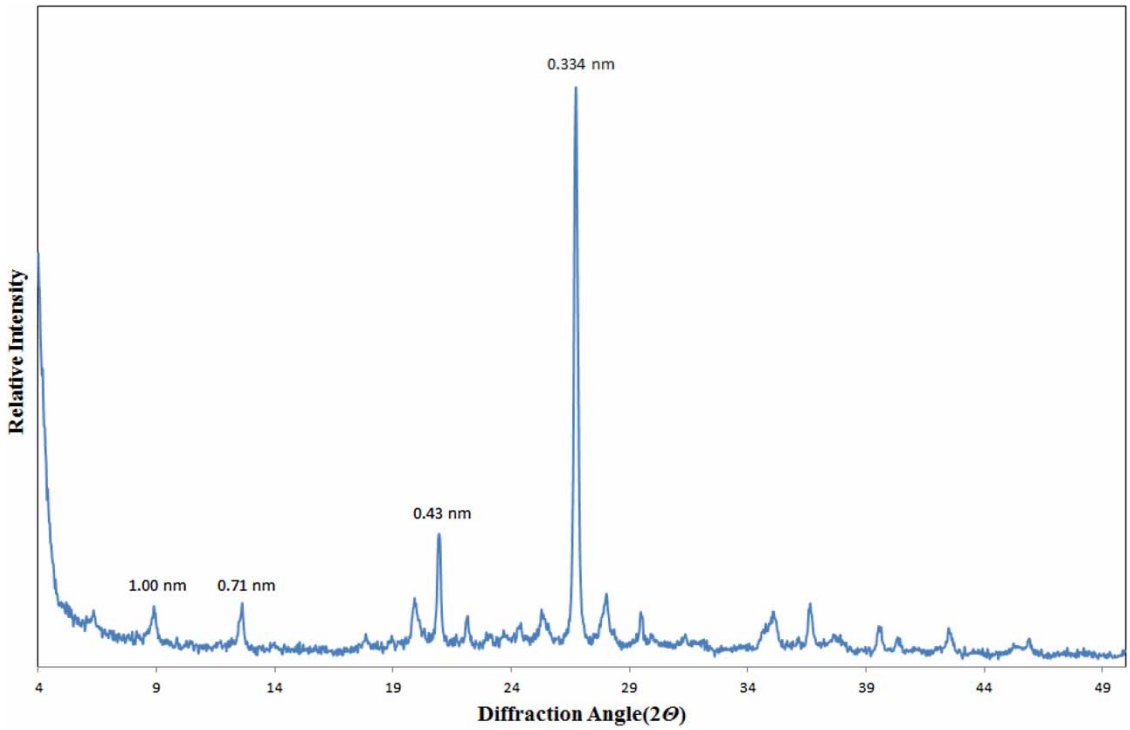


**Figure 2** | XRD spectra of the canal sediment.

**Table 1** | Results of TCLP test for the canal sediment

| Metal | TCLP | Standard Level |
|---|---|---|
| Cr | ND | 5.0 |
| Cu | 13.0 ± 0.8 | 15.0 |
| Cd | ND | 1.0 |
| Ni | 77.1 ± 0.1 | – |
| Pb | ND | 5.0 |
| Zn | 310 ± 0.2 | – |
| As | ND | 5.0 |
| Hg | ND | 0.2 |

Unit: mg $L^{-1}$.
–: Not defined.

following MB sorption investigations were conducted at an optimal pH level of 8.0.

## Adsorption kinetics

### Effects of initial MB concentration

Figure 5(a) illustrates time profiles of MB adsorption by the canal sediment for different initial concentrations of MB. $C_0$ denotes the initial MB concentration in the aqueous phase (mg $L^{-1}$), and $C_t$ denotes the MB concentration in the aqueous phase at time t. The value of $C_t/C_0$ can be considered as a measure of MB removal that decreases with increased MB removal. As shown in Figure 5(a), MB adsorption is very fast in the initial 20 min, but solutions with higher initial MB concentrations show poor removal ratios. The efficiency of MB removal by the canal sediment follows the trend of 100 mg $L^{-1}$ (98.5%) >200 mg $L^{-1}$ (93.3%) >300 mg $L^{-1}$ (74.5%) >400 mg $L^{-1}$ (61.5%) >500 mg $L^{-1}$ (57.7%) at adsorption steady state. Only the pseudo-second-order adsorption equation fits the experimental data well and shows high correlations (Figure 5(b) and Table 3). The pseudo-second-order adsorption rate constants, $k_2$, for the 100, 200, 300, 400, and 500 mg $L^{-1}$ MB solutions are 0.0718, 0.0099, 0.0053, 0.0046, and 0.0021 g $mg^{-1}$ $min^{-1}$, respectively. Higher MB concentration in the suspension seems to reduce the diffusion of the MB molecule in the boundary layer of the sediment particles, which decreases the adsorption rate.

On the other hand, the time profiles of the concentration effect are useful for developing a wastewater dye processing scheme using the batch method. An example of how to use the time profiles is depicted in Figure 6 and explained as follows. Analyzing the time profiles in Figure 5(a), the removal ratios of MB for the 500, 300, and

**Table 2** | Dissolution amounts of heavy metals from the canal sediment when it was mixed vigorously with aqueous solution at pH 2 to pH 10

| Metal | pH2 | pH3 | pH4 | pH5 | pH6 | pH7 | pH8 | pH9 | pH10 | Discharge Standard |
|---|---|---|---|---|---|---|---|---|---|---|
| Cr | 0.26 ± 0.04 | ND | ND | ND | ND | ND | ND | ND | ND | <2 |
| Cu | 6.35 ± 0.44 | 0.07 ± 0.01 | 0.05 ± 0.01 | 0.05 ± 0.01 | 0.04 ± 0.00 | 0.04 ± 0.01 | 0.04 ± 0.00 | 0.05 ± 0.00 | 0.04 ± 0.00 | <3 |
| Cd | ND | ND | ND | ND | ND | ND | ND | ND | ND | <0.03 |
| Ni | 2.19 ± 0.08 | 0.03 ± 0.01 | ND | ND | ND | ND | ND | ND | ND | <1 |
| Pb | ND | ND | ND | ND | ND | ND | ND | ND | ND | <1 |
| Zn | 13.5 ± 0.35 | 0.50 ± 0.06 | ND | ND | ND | ND | ND | ND | ND | <5 |
| As | ND | ND | ND | ND | ND | ND | ND | ND | ND | <0.5 |
| Hg | ND | ND | ND | ND | ND | ND | ND | ND | ND | <0.005 |

Unit: mg $L^{-1}$.

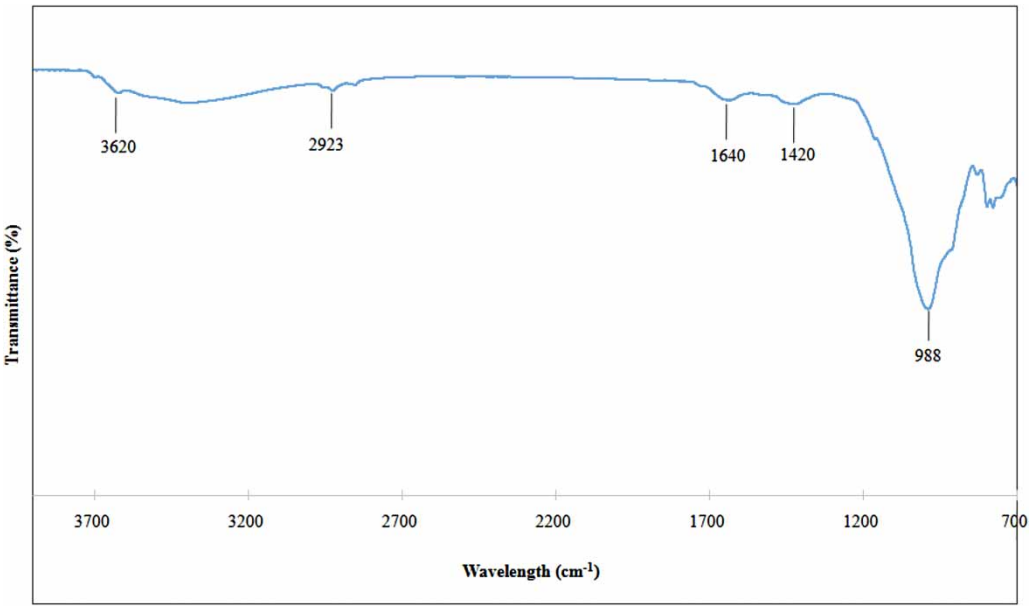


**Figure 3** | FT-IR spectra of the canal sediment.

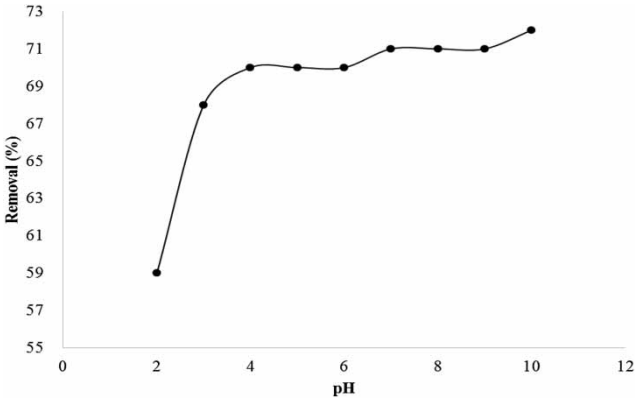


**Figure 4** | The removal efficiency of MB by canal sediment adsorption treatment at various pH values.

100 mg $L^{-1}$ treatments at 30 min of reaction time are about 43, 63, and 97%, respectively. Assuming 1 ton of MB wastewater with an initial concentration of 500 mg $L^{-1}$, the wastewater can be introduced into a first reaction tank and 5 kg of canal sediment particles (140–200 mesh) then can be added to the tank. As expected, the MB concentration of the suspension will decline to 331 mg $L^{-1}$ in 30 min. Then, this suspension can be introduced into a second tank and the same operation repeated. The MB concentration will decrease to about 108 mg $L^{-1}$ in this stage. Finally, the suspension is introduced into a third tank and treated again. In this tank, the MB concentration would be reduced to only 4 mg $L^{-1}$. Thus, it is possible to purify a

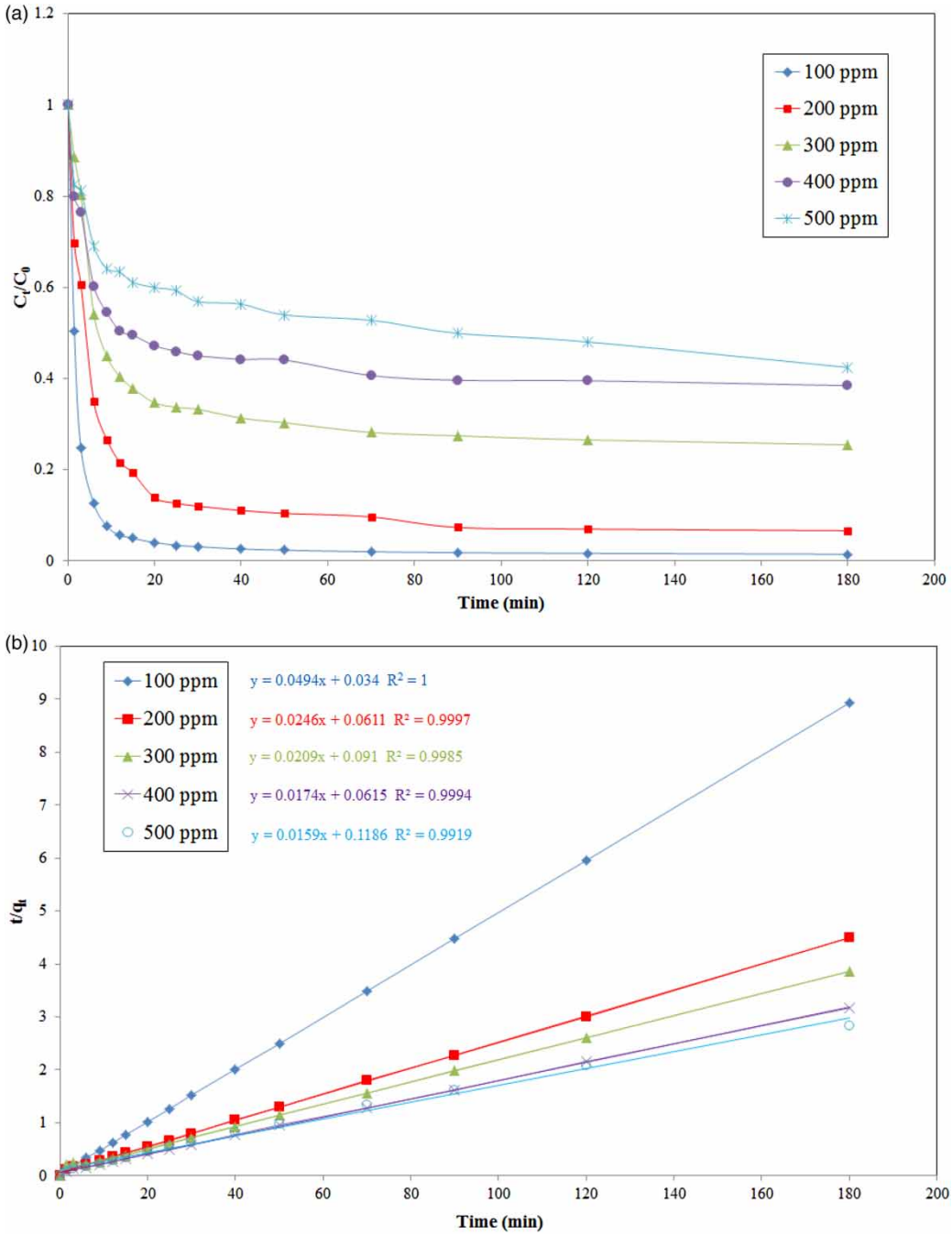


**Figure 5** | Time profiles of (a) MB adsorption and (b) pseudo-second-order kinetic model for canal sediment with different initial concentrations of MB (dosage = 4.98 g $L^{-1}$, 140–200 mesh, pH = 8.0, T = 25 °C).

high-concentration MB solution well using the canal sediment within a short time.

## Effects of temperature and activation energy

Time profiles for the different MB concentrations are depicted at different temperatures of canal sediment (140–200 mesh) in Figure 7(a). A higher temperature treatment with the sediment produces higher removal efficiency, but the differences in MB removal between the different temperature treatments are quite small, except for the one conducted at 10 °C. According to the kinetic models for the different temperature treatments, only the pseudo-second-order equation shows a very high correlation

**Table 3** | Determination constants ($r^2$) and rate constants of pseudo-second-order ($k_2$) models at different temperatures, initial MB concentration, and particle sizes of canal sediment

| Treatment | $R^2$ 1st order | $R^2$ 2nd order | $R^2$ Elovich | Rate Constant $k_2$ (g mg$^{-1}$ min$^{-1}$) | Activation Energy $E_a$ (kJ mole$^{-1}$) |
|---|---|---|---|---|---|
| Temperature | | | | | |
| 10°C | 0.743 | 0.996 | 0.920 | 0.0030 | 16.434 |
| 25°C | 0.781 | 0.998 | 0.866 | 0.0048 | |
| 40°C | 0.773 | 0.999 | 0.815 | 0.0071 | |
| 55°C | 0.800 | 0.999 | 0.775 | 0.0077 | |
| Concentration | | | | | |
| 100 ppm | 0.828 | 0.999 | 0.608 | 0.0718 | |
| 200 ppm | 0.866 | 0.999 | 0.826 | 0.0099 | |
| 300 ppm | 0.781 | 0.998 | 0.866 | 0.0053 | |
| 400 ppm | 0.767 | 0.999 | 0.866 | 0.0046 | |
| 500 ppm | 0.580 | 0.991 | 0.935 | 0.0021 | |
| Particle Size | | | | | |
| 50–100 mesh | 0.896 | 0.998 | 0.969 | 0.0015 | |
| 100–140 mesh | 0.879 | 0.999 | 0.897 | 0.0039 | |
| 140–200 mesh | 0.889 | 0.998 | 0.866 | 0.0048 | |
| >200 mesh | 0.833 | 0.999 | 0.849 | 0.0046 | |

coefficient ($r^2$ ranged from 0.996 to 0.999) (Figure 7(b) and Table 3). The calculated adsorption rate constants, $k_2$ (g mg$^{-1}$ min$^{-1}$), increase with increasing temperature, indicating that high temperature accelerates the adsorption equilibrium of the canal sediment for MB.

The Arrhenius equation was employed to calculate the activation energy ($E_a$) and the pre-exponential factor (Moore & Pearson 1981):

$$k = Ae^{-Ea}/RT \tag{10}$$

After linearizing, the Arrhenius equation becomes

$$lnk = lnA - E_a/RT \tag{11}$$

where $k$ is the rate coefficient, $A$ is the frequency factor, $E_a$ is the Arrhenius activation energy, $R$ is the universal gas constant (8.314 J mol$^{-1}$ K$^{-1}$), and $T$ is the absolute temperature ($K$). The activation energy and frequency factor can be calculated from the slope and intercept of the plot of $ln\ k$ vs. $1/T$. From the pseudo-second-order rate constant, $k_2$, in Table 3, the activation energy determined using the Arrhenius equation for MB adsorption on the canal sediment is 16.434 kJ mol$^{-1}$. Sparks (1986) proposed that values of $E_a$ higher than 42 kJ mol$^{-1}$ indicate a chemically controlled reaction process and that lower values represent a diffusion-controlled process. We conclude that a diffusion-controlled process is the rate-limiting step and that physisorption is the dominant adsorption mechanism for MB adsorption by the canal sediment.

## Effects of the particle size

As shown in Figure 8(a), the 100–140 mesh treatment presented the highest MB removal rate (86.3%). Other treatments showed lower but nearly identical removal levels ranging from 72.4% to 76.6%. Although the 50–100 mesh treatment showed slow adsorption in the early stages, the removal level of this treatment caught up with those of the other two treatments at 60 min. Based on actual observation, the 50–100 mesh sediment, which had a weaker aggregate structure, gradually collapsed into smaller pieces with vigorous shaking, and this result may have increased the total surface area for adsorption. The organic matter contents of the 50–100, 100–140, 140–200, and 200–350 mesh sediments were 10.5, 13.5, 10.7, and 7.2%, respectively. Clearly, the organic matter content dominates the MB adsorption, not the factor of actual specific surface area. The pseudo-second-order equation showed a better correlation ($r^2$ ranging from 0.998 to 0.999) than both the pseudo-first-order equation ($r^2$ from 0.894 to 0.979) and the Elovich equation ($r^2$ from 0.833 to 0.896) (Figure 8(b) and Table 3). Therefore, only the pseudo-second-order equation was used for the kinetic study. The calculated adsorption rate constants, $k_2$ (g mg$^{-1}$ min$^{-1}$), for the pseudo-second-order equation are 0.0015, 0.0039, 0.0048, and 0.0046 for the 50–100, 100–140, 140–200, and 200–350 mesh treatments, respectively. We found that the time to adsorption equilibrium dominates the size of the value of $k_2$ but not the amount of MB removed. Analyzing the time profiles, the 50–100 mesh treatment presented

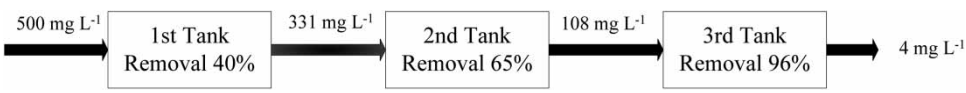


**Figure 6** | An example application of the time profiles for various initial concentrations of MB to wastewater treatment (dosage = 5 g L$^{-1}$, 140–200 mesh, pH = 8.0, T = 25 °C).

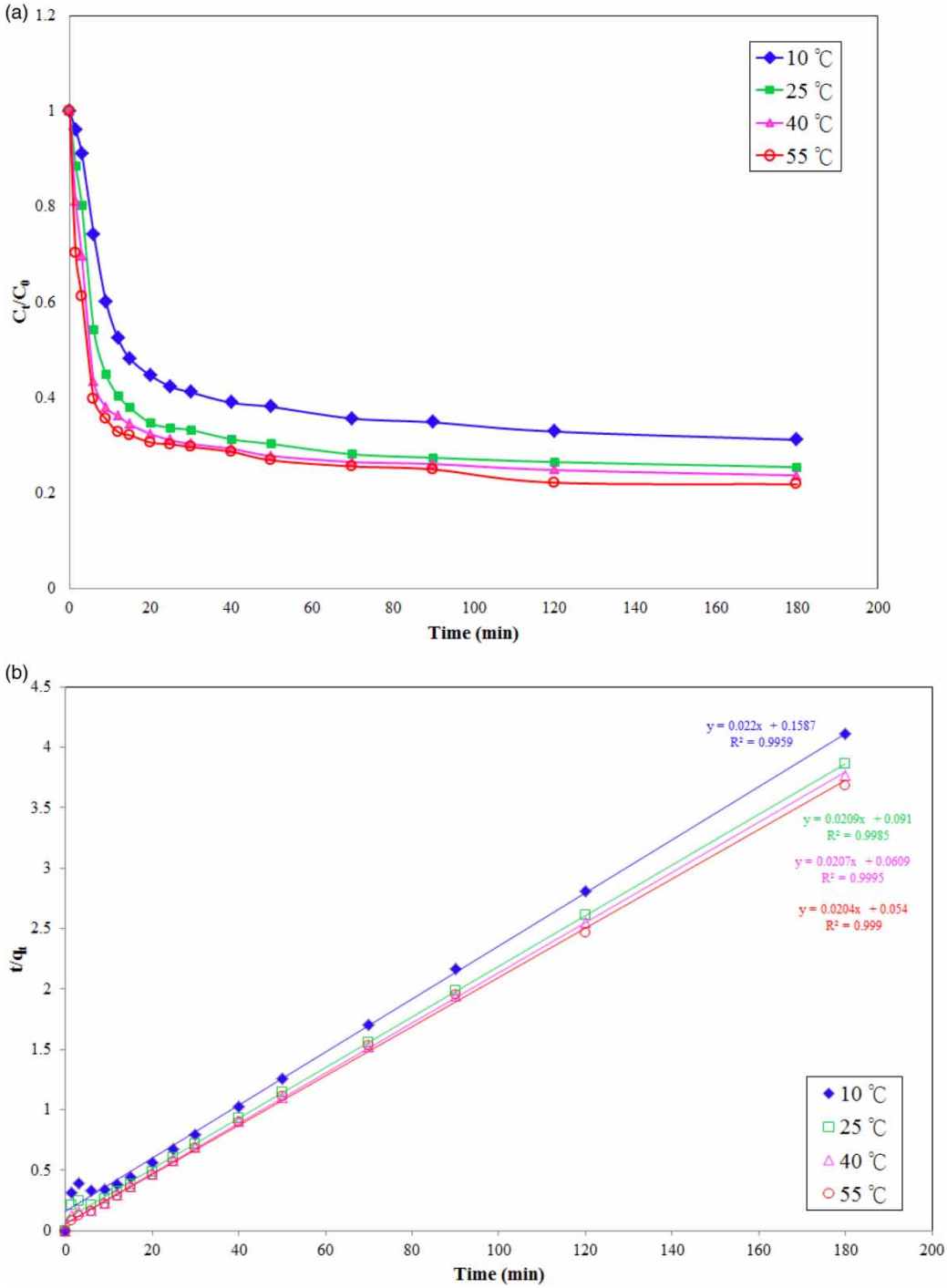


**Figure 7** | Time profiles of (a) MB adsorption and (b) pseudo-second-order kinetic model by canal sediment WPWS at different temperatures ($C_o$ = 300 mg $L^{-1}$, 140–200 mesh, dosage = 4.98 g $L^{-1}$, pH = 8.0).

relatively slow adsorption in the early stages, but MB adsorption reached a steady state at around 180 min. The 100–140 mesh treatment showed better adsorption in the whole process, and MB adsorption also approached a steady state near 180 min. A sorbent rich in organic matter generally provides more sites for sorption, which may extend the reaction time. These factors result their low $k_2$ values (Table 3).

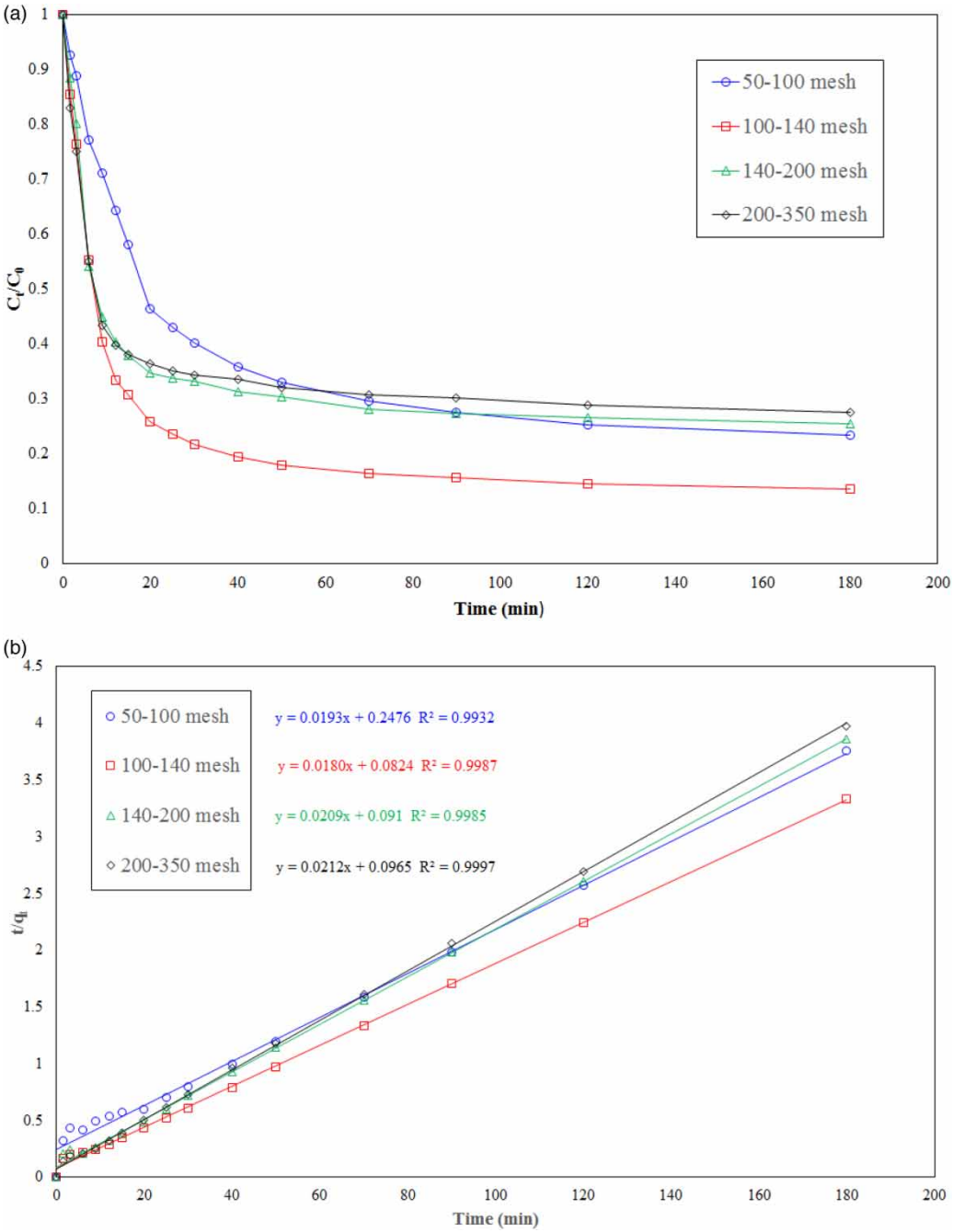


**Figure 8** | Time profiles of (a) MB adsorption and (b) pseudo-second-order kinetic model by canal sediment with different particle sizes ($C_0 = 300$ mg L$^{-1}$, dosage = 4.98 g L$^{-1}$, pH = 8.0, T = 25 °C).

## Temperature effect versus the isotherms

As listed in Table 4, the temperature change seemed to influence the behavior of MB adsorption substantially. Compared to other isotherms, the Freundlich isotherm fitting attains the lowest correlation at the lowest temperature (10 °C), but it attains the highest correlations in the intermediate temperature conditions (25 and 40 °C). Furthermore, all the isotherms were found to not fit the experimental data well at 55 °C ($r^2$ ranged from 0.785 to 0.898). Therefore, the related constants, factors, and parameters, including $Q_m$, $K_L$, $K_F$, $A_T$, $q_s$, and $K_{DR}$, are valueless. We speculate that the organic matter in the canal sediment became unstable at high temperature

**Table 4** | Calculated isotherm parameters and determination constants for MB adsorption by the canal sediment

| Temp | Langmuir | | | Freundlich | | | Temkin | | | Dubinin–Radushkevich | | | |
|---|---|---|---|---|---|---|---|---|---|---|---|---|---|
| (°C) | $Q_m$ (mg g$^{-1}$) | $K_L$ (L mg$^{-1}$) | $R^2$ | $K_F$ | $n$ | $R^2$ | $b_T$ (J mole$^{-1}$) | $A_T$ (L g$^{-1}$) | $R^2$ | $q_s$ (mg g$^{-1}$) | $K_{DR}$ (mole$^2$ kJ$^{-2}$) | $E$ (kJ mole$^{-1}$) | $R^2$ |
| 10 | 56.0 | 0.4 | 0.972 | 3.7 | 4.5 | 0.960 | 89,010 | 2,527 | 0.976 | 62.0 | 7.0E-09 | 8,453 | 0.976 |
| 25 | 57.5 | 0.6 | 0.951 | 3.8 | 4.4 | 0.990 | 86,629 | 2,666 | 0.967 | 65.6 | 5.8E-09 | 9,315 | 0.967 |
| 40 | 57.5 | 0.7 | 0.939 | 3.8 | 4.4 | 0.992 | 89,727 | 2,822 | 0.951 | 66.1 | 5.0E-09 | 10,018 | 0.951 |
| 55 | 66.3 | 0.6 | 0.898 | 4.2 | 5.8 | 0.785 | 121,554 | 17,192 | 0.804 | 66.2 | 3.7E-09 | 11,685 | 0.804 |

and that its conformation became looser and soft. Liu *et al.* (2012b) found that the amount of organic carbon dissolved out of WPWS during the adsorption reaction was two times higher at 50 °C than at 10 °C. Leboeuf & Weber (1997) revealed water-wet humic acid has a polymer-like characteristic and that its structure expands at temperature higher than 43 °C. Both $Q_m$ and $q_s$ increase with temperature increase from 10 to 55 °C. Therefore, it can be concluded that canal sediment shows better adsorptive capacities for MB at higher temperature. In addition, all $q_s$ values (ranging from 62.0 to 66.1 mg g$^{-1}$) are higher than $Q_m$ values (ranging from 56.0 to 57.7 mg g$^{-1}$). We are convinced that the $q_s$ values are more available because they produce better fitting results. The Dubinin–Radushkevich isotherm model is more favorable for the adsorption. After all, the canal sediment particles have a quite heterogeneous surface. Table 5 presents the comparison of adsorption capacity of canal sediment from the Langmuir isotherm for MB with that of various industrial and agricultural wastes reported in literatures. Although the $Q_m$ level of the canal sediment was not as high as that of other materials, we assessed that using the sediment to remove MB would still be highly cost-effective because of its abound source, the requirement for little processing for its use, and the simplicity of application.

Gibbs free energy ($\Delta G^\circ$) and enthalpy ($\Delta H^\circ$) are calculated using the van 't Hoff thermodynamic equations (Liu *et al.* 2012b). The $\Delta G^\circ$ values derived from the isotherm experiments are −27.6, −30.1, and −32.0 kJ mol$^{-1}$ at 10, 25, and 40 °C, respectively, indicating that the adsorption processes of MB for the canal sediment are spontaneous reactions under the experimental conditions. The interaction between MB and the canal sediment can be regarded as physical sorption (Jaycok & Parfitt 1981). The calculated values of enthalpy ($\Delta H^\circ$) and entropy ($\Delta S^\circ$) are 14.6 kJ mol$^{-1}$ and 149.2 kJ mol$^{-1}$, respectively. The positive sign of $\Delta H^\circ$ shows that the sorption of MB by the canal sediment is endothermic, and the positive value of $\Delta S^\circ$ indicates a higher tendency of disorder at the interface between the canal sediment and MB in the solutions. According to these observations, the MB–sediment suspension system is

**Table 5** | Adsorption capacities of various adsorbents for MB

| Adsorbents | pH | Temp. °C | $Q_m$ (mg g$^{-1}$) | Reference |
|---|---|---|---|---|
| Canal sediment | 8.0 | 10 | 56.0 | This work |
| Sulfonated tea waste | 10.0 | 25 | 1,008 | Ahsan *et al.* (2018) |
| Waste tire rubber | 10.0 | 23 | 833 | Islam *et al.* (2018) |
| Citrus limetta peel | 8.0 | 25 | 227 | Shakor & Nasar (2016) |
| Fish scale activated material | 11.0 | 30 | 184 | Marrakchi *et al.* (2017) |
| Magnetized palm shell-waste based activated carbon | 7.0 | NP | 163 | Wong *et al.* (2016) |
| Tea waste | 8.0 | 25 | 85.2 | Uddin *et al.* (2009) |
| Leaves of solanum tuberosum | 7.0 | 30 | 52.6 | Gupta *et al.* (2016) |
| Empty fruit bunch | NP | 30 | 50.8 | Rebitanim *et al.* (2012) |
| (Corn stalk/organic montmorillonite) hydrogel composite | 7.0 | 50 | 49.0 | Ma *et al.* (2017a, 2017b) |
| Pig manure | 6.5 | 25 | 25.0 | Lonappan *et al.* (2016) |

NP: not reported.

spontaneous and high temperature favors MB adsorption by the canal sediment.

## CONCLUSIONS

The canal sediment is an effective adsorbent of MB in solutions due to its characteristic of high organic matter content. Carboxyl groups are the prominent functional groups interacting with MB. When canal sediment is utilized as an adsorbent, the adsorption reaction should be conducted at pH higher than 3.0 to prevent massive dissolution of Cu, Zn, and Ni. In the isotherm study, the MB adsorption seemed to be well described by the Freundlich isotherm equation, exclusive of the reaction at 55 °C. High temperature favors MB adsorption, and the reaction is spontaneous and endothermic. Nevertheless, the MB adsorption presents an abnormal behavior at the highest temperature, according to its low correlation relationship to all isotherms ($R^2$ ranged from 0.785 to 0.898). We speculate that this behavior is caused by the change in organic conformation of the sediment, which becomes looser in a hyperthermal situation. The calculated maximum adsorption capacities for the Langmuir isotherm and the Dubinin–Radushkevich isotherm at 25 °C are 57.5 and 65.5 mg $g^{-1}$, respectively. According to the adsorption kinetics, only the pseudo-second-order sorption equation fits the experimental results well. A higher initial concentration of MB results in a decrease in the adsorption rate of external diffusion. The 100–140 mesh sediment shows the largest adsorption capacity because of its highest organic content. Organic matter content dominates the MB adsorption, rather than the factor of specific surface area.

To avoid flooding in the rainy season, regular canal dredging is necessary in Taiwan. Several megatons of sediments are, therefore, regularly dug up and in need for disposal. Most of them are taken to a sanitary landfill site or incinerator. Here, we propose a way to reuse these sediments before such disposals. As demonstrated by the results of this study, these sediments may become the source of the required adsorbent. Only a sediment with high organic content is suitable as adsorbent in dye-wastewater treatment. In general, such sediments are black or dark in color. If the sediment is obtained from a canal that has only received domestic sewage, it may not require special pretreatment before use. By simply processing via air-drying, disintegration, grounding, and sieving, the sediment can be applied to dye adsorption directly. If the sediment is obtained from a canal that has received industrial wastewater discharge over the long term, its usage will be limited due to the possibility of its being contaminated with toxic substances.

The high correlation of the adsorption behavior indicates that the MB removal can be predicted precisely by the model, and this is beneficial for actual application. Using the canal sediment for purification of dye-containing wastewater has several advantages, including it being a simple technique, having low cost and good capacity, and requiring little processing. It is suggested that the canal sediment adsorption process is suitable for serving as an auxiliary treatment in a traditional wastewater treatment process under good situations. For example, conducting it before the activated carbon adsorption can decrease the loading and reduce the operating costs of the latter process (Figure 9). On the other hand, the canal sediment is also recommended for clarifying the dye wastewater in a small factory that does not have good disposal equipment. The precipitated canal sediment particles are not difficult to collect from the reaction tank after the water purification process. Nevertheless, the used sediment is not worth recovering or regenerating due to the economic burden of doing so. When the collected particles are sent to a cement factory or brick kiln factory for final disposal, the Si, Al, and Ca in the canal sediment will serve as raw materials for making

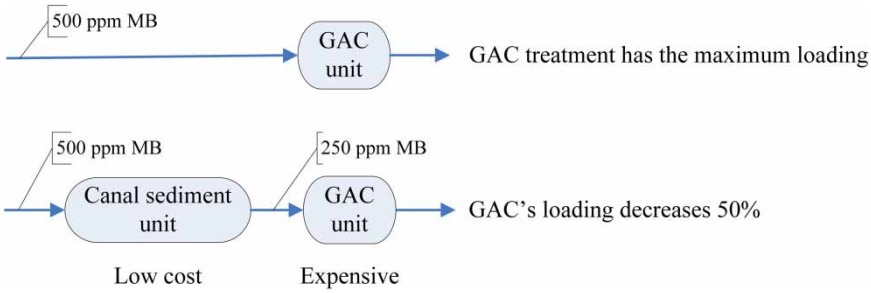


**Figure 9** | An example application of the canal sediment as an auxiliary process decreasing the loading of activated carbon in a wastewater treatment.

the cement or bricks. We believe that the MB trapped on the canal sediment particles will be degraded and disappear, following the organic matter, during the super-high-temperature calcination process.

## ACKNOWLEDGEMENTS

This work was financially supported by the National Science Council, Taiwan, Republic of China, under projects NSC 103-2313-B-197 -001-.

## REFERENCES

Ahsan, Md. A., Katla, S. K., Lslam, Md. T., Hernandez-Viezcas, J. A., Martinez, L. M., Diaz-Moreno, C. A., Lopez, J., Singamaneni, S. R., Banuelos, J., Gardea-Torresdey, J. & Noveron, J. C. 2018 Adsorptive removal of methylene blue, tetracycline and Cr(VI) from water using sulfonated tea waste. *Environmental Technology & Innovation* **11**, 23–40.

Akazdam, S., Chafi, M., Yassine, W. & Gourich, B. 2017 Removal of acid orange 7 dye from aqueous solution using the exchange resin amberlite FPA-98 as an efficient adsorbent: kinetics, isotherms, and thermodynamics study. *Journal of Materials and Environmental Sciences* **8** (8), 2993–3012.

Aroguz, A. Z., Gulen, J. & Evers, R. H. 2008 Adsorption of methylene blue from aqueous solution on pyrolyzed petrified sediment. *Bioresource Technology* **99** (6), 1503–1508.

Bhatti, H. N., Jabeen, A., Iqbal, M., Noreen, S. & Naseem, Z. 2017 Adsorptive behavior of rice bran-based composites for malachite green dye: isotherm, kinetic and thermodynamic studies. *Journal of Molecular Liquids* **237**, 322–333.

Benjelloun, Y., Lahrichi, A., Boumchita, S., Idrissi, M., Miyah, Y., Anis, K., Nenov, V. & Zerrouq, F. 2017 Removal of crystal violet by wet oxidation with $H_2O_2$ over an iron oxide catalyst synthesized from fly ash. *Journal of Materials and Environmental Sciences* **8** (7), 2259–2269.

Chung, K. T. & Cerniglia, C. E. 1992 Mutagenicity of azo dyes: structure-Activity relationships. *Mutation Research/Review in Genetic Toxicology* **277** (3), 201–220.

Dabrowski, A. 2001 Adsorption — from theory to practice. *Advance in Colloid and Interface Science* **93** (1), 135–224.

Franca, A. S., Oliveira, L. S. & Ferreira, M. E. 2009 Kinetics and equilibrium studies of methylene blue by spent coffee grounds. *Desalination* **249** (1), 267–272.

Gerasimowicz, W. V. & Byler, D. M. 1985 Carbon-13 CPMAS NMR and FT-IR spectroscopic studies of humic acids. *Soil Science* **139**, 270–278.

Gerçel, Ö. 2016 Removal of textile dye from aqueous solution by electrochemical method. *Separation Science and Technology* **51** (4), 711–717.

Gunay, A., Arslankaya, E. & Tosun, I. 2007 Lead removal from aqueous solution by natural and pretreated cinoptilolite adsorption equilibrium and kinetics. *Journal of Hazardous Materials* **146** (1–2), 362–371.

Gupta, N., Kushwaha, A. K. & Chattopadhyaya, M. C. 2016 Application of potato (*Solanum tuberosum*) plant wastes for the removal of methylene blue and malachite green dye from aqueous solution. *Arabian Journal of Chemistry* **9** (1), S707–S716.

Hagvall, K., Persson, P. & Karlsson, T. 2015 Speciation of aluminum in soils and stream waters: the importance of organic matter. *Chemical Geology* **417** (6), 32–43.

Islam, Md. T., Saenz-Arana, R., Hernandez, C., Guinto, T., Ahsan, Md. A., Bragg, D. T., Wang, H., Alvarado-Tenorio, B. & Noveron, J. C. 2018 Conversion of waste tire rubber into a high-capacity adsorbent for the removal of methylene blue, methyl orange, and tetracycline from water. *Journal of Environmental Chemical Engineering* **6** (2), 3070–3082.

Jaycok, M. J. & Parfitt, G. D. 1981 Introduction to interfaces and the forces involved in their formation. In: *Chemistry of Interfaces* (C. H. Bamford & J. Burgess, eds). Ellis Horwood, West Sussex, UK.

Leboeuf, E. J. & Weber Jr, W. J.. 1997 A distributed reactivity model for sorption by soils and sediments. 8. sorbent organic domains: discovery of a humic acid glass transition and an argument for a polymer-based model. *Environmental Science & Technology* **31** (6), 1697–1702.

Liu, C. C., Li, Y. S., Chen, Y. M., Li, H. H. & Wang, M. K. 2012a Removal of methylene blue from aqueous solution using wine-processing waste sludge. *Water Science & Technology* **65** (12), 2191–2199.

Liu, C. C., Chen, Y. M., Wang, M. K. & Lin, Y. A. 2012b Adsorption of Cu(II) from aqueous solution by wine-processing waste sludge. *Water Environment Research* **84** (9), 733–743.

Lonappan, L., Rouissi, T., Das, R. K., Brar, S. K., Ramirez, A. A., Verma, M., Surampalli, R. Y. & Valero, J. R. 2016 Adsorption of methylene blue on biochar microparticles derived from different waste materials. *Waste Management* **49**, 537–544.

Ma, D., Zhu, B., Cao, B., Wang, J. & Zhang, J. 2017a Fabrication of the novel hydrogel based on waste corn stalk for removal of methylene blue dye from aqueous solution. *Applied Surface Science* **422**, 944–952.

Ma, X., Chen, P., Zhou, M., Zhong, Z., Zhang, F. & Xing, W. 2017b Tight ultrafiltration ceramic membrane for separation of dyes and mixed salts (both $NaCl/Na_2SO_4$) in textile wastewater treatment. *Industrial & Engineering Chemistry Research* **56** (24), 7070–7079.

Marrakchi, F., Auta, M., Khanday, W. A. & Hameed, B. H. 2017 High-surface-area and nitrogen-rich mesoporous carbon material from fishery waste for effective adsorption of methylene blue. *Powder Technology* **321**, 428–434.

Miralles, I., van Wesemael, B., Cantón, Y., Chamizo, S., Ortega, R., Domingo, F. & Almendros, G. 2012 Surrogate descriptors of C-storage processes on crusted semiarid ecosystems. *Geoderma* **189–190**, 227–235.

Molla, M. A. I., Furukawa, M., Tateishi, I., Katsumata, H., Suzuki, T. & Kaneco, S. 2017 Photocatalytic decolorization of dye with self-dye-sensitization under fluorescent light irradiation. *Chemengineering* **1** (8), 1–10.

Moore, J. W. & Pearson, R. G. 1981 *Kinetic and Mechanism*, 3rd edn. John Wiley & Sons, New York, NY, USA.

Mouni, L., Belkhiri, L., Bollinger, J., Bouzaza, A., Assadi, A., Tirri, A., Dahmoune, F., Madani, K. & Remini, H. 2018 Removal of Methylene Blue from aqueous solutions by adsorption on Kaolin: kinetic and equilibrium studies. *Applied Clay Science* **153** (1), 38–45.

Mukhlish, M. Z. B., Khan, M. M. R., Islam, A. R. & Akanda, A. N. M. S. 2016 Removal of reactive dye from aqueous solution using coagulation–flocculation coupled with adsorption on papaya leaf. *Journal of Mechanical Engineering and Sciences* **10** (1), 1884–1894.

Nausheen, S., Bhatti, H. N., Hanif, M. A. & Khalil-ur Rehman. 2017 Enhanced removal of golden XGL dye by clay composites: batch and column studies. *Polish Journal of Environmental Studies* **26** (5), 2113–2123.

Rebitanim, N. Z., Ghani, W. A. W. A. K., Mahmoud, D. K., Rebitanim, N. A. & Salleh, M. A. M. 2012 Adsorption capacity of raw empty fruit bunch biomass onto methylene blue dye in aqueous solution. *Journal of Purity, Utility Reaction and Environment* **1** (1), 45–60.

Reddy, P. M. K., Verma, P. & Subrahmanyam, C. 2016 Bio-waste derived adsorbent material for methylene blue adsorption. *Journal of the Taiwan Institute of Chemical Engineers* **58**, 500–508.

Rhoades, J. D. 1982 Cation exchange capacity. In: *Methods of Soil Analysis. Part 2. Agronomy Monograph 9*, 2nd edn (A. L. Page, R. H. Miller & D. R. Keeny, eds). ASA and SSSA, Madison, WI, USA, pp. 149–157.

Shakor, S. & Nasar, A. 2016 Removal of methylene blue dye from artificially contaminated water using *Citrus limetta* peel waste as a very low cost adsorbent. *Journal of the Taiwan Institute of Chemical Engineers* **66**, 154–163.

Sham, A. Y. W. & Notley, S. M. 2018 Adsorption of organic dyes from aqueous solutions using surfactant exfoliated grapheme. *Journal of Environmental Chemical Engineering* **6** (1), 495–504.

Shoukat, S., Bhatti, H. N., Iqbal, M. & Noreen, S. 2017 Mango stone biocomposite preparation and application for crystal violet adsorption: a mechanistic study. *Microporous and Mesoporous Materials* **239**, 180–189.

Sparks, D. L. 1986 Kinetics of reactions in pure and mixed systems. In: *Soil Physical Chemistry* (D. L. Sparks, ed.). CRC Press, Boca Raton, FL, USA, pp. 83–146.

Sun, Q. & Yang, L. 2003 The adsorption of basic dyes from aqueous solution on modified peat–resin particle. *Water Research* **37** (7), 1535–1544.

Uddin, Md. T., Lslam, Md. A., Mahmud, S. & Rukanuzzaman, Md. 2009 Adsorptive removal of methylene blue by tea waste. *Journal of Hazardous Materials* **164** (1), 53–60.

Waranusantigul, P., Pokethitiyook, P., Kruatrachue, M. & Upatham, E. S. 2003 Kinetics of basic dye (methylene blue) biosorption by giant duckweed (*Spirodela polyrrhiza*). *Environmental Pollution* **125** (3), 385–392.

Weng, C. H., Lin, W. T. & Tzeng, T. W. 2009 Removal of methylene blue from aqueous solution by onto pineapple leaf powder. *Journal of Hazardous Materials* **170** (1), 417–424.

White, J. L. & Roth, C. B. 1982 Infrared spectrometry. In: *Methods of Soil Analysis. Part 1. Agronomy Monograph 9*, 2nd edn (A. Klute, ed.). ASA and SSSA, Madison, WI, USA, pp. 291–330.

Wong, K. T., Eu, N. C., Lbrahim, S., Kim, H., Yoon, Y. & Jam, M. 2016 Recyclable magnetite-loaded palm shell-waste based activated carbon for the effective removal of methylene blue from aqueous solution. *Journal of Cleaner Production* **115**, 337–342.

First received 7 February 2018; accepted in revised form 12 July 2018. Available online 26 July 2018